Proceedings of the 2005 IEEE
International Conference on Robotics and Automation
Barcelona, Spain, April 2005

Design Considerations for Robotic Needle Steering*

Robert J. Webster III, Jasenka Memisevic, and Allison M. Okamura
Department of Mechanical Engineering
Engineering Research Center for Computer-Integrated Surgical Systems and Technology
The Johns Hopkins University
Baltimore, MD, 21218 USA
robert.webster@jhu.edu, memisej@slu.edu, aokamura@jhu.edu

***Abstract*— Many medical procedures involve the use of needles, but targeting accuracy can be limited due to obstacles in the needle's path, shifts in target position caused by tissue deformation, and undesired bending of the needle after insertion. In order to address these limitations, we have developed robotic systems that actively steer a needle in soft tissue. A bevel (asymmetric) tip causes the needle to bend during insertion, and steering is enhanced when the needle is very flexible. An experimental needle steering robot was designed that includes force/torque sensing, horizontal needle insertion, stereo image data acquisition, and controlled actuation of needle rotation and translation. Experiments were performed with a phantom tissue to determine the effects of insertion velocity and bevel tip angle on the needle path, as well as the forces acting on the needle during insertion. Results indicate that needle steering inside tissue does not depend on insertion velocity, but does depend on bevel tip angle. In addition, the forces acting on the needle are directly related to the insertion velocity.**

***Index Terms*— Keywords: medical robotics, needle steering, nonholonomic systems.**

I. Introduction

Needle insertion is an important aspect of many medical diagnoses and treatments, particularly percutaneous procedures requiring therapy delivery to or sample removal from a specific location. However, errors in needle targeting can mitigate the effectiveness of diagnosis or therapy. Biopsies, for example, cannot completely rule out malignancy due to inaccuracy in positioning the needle tip. Also, radioactive seeds in procedures such as prostate brachytherapy are often placed at locations substantially different than those pre-planned for optimal dosage.

Needle steering has the potential to correct targeting errors and steer around obstacles to reach previously inaccessible locations. Control and planning based on a steering model can compensate for targeting disturbances due to needle bending, error in insertion angle, and tissue deformation. In this paper, we focus on the design of two different devices for steerable needle insertion, as well as experiments to determine the effect of needle insertion velocity and bevel tip angle on needle path.

*This work is partially supported by NIH Grant #R21-EB003452 to A. M. Okamura, an NDSEG fellowship to R. J. Webster III, and NSF Grant #EEC-9731478 for an REU fellowship to J. Memisevic.

In our systems, the steering effect is caused by the asymmetry of a bevel tip on a flexible needle [9], [11]. Lateral motion and tissue deformation can also cause steering, although our systems do not explicitly employ those techniques. Clinically, needles are manually steered through a combination of lateral, twisting, and inserting motions under visual feedback from imaging systems such as ultrasound [13]. However, these techniques can yield inconsistent results and are difficult to learn. Physicians also sometimes continually spin bevel tip needles during insertion to *prevent* them from bending.

A. Previous Work

The effect of needle bending for the purpose of steering has recently been explored by several groups. Examples of canula-based steering methods include the use of a pre-bent stylus inside a straight canula [6] and a telescoping double canula where the internal canula is pre-bent [4]. DiMaio and Salcudean [5] formulate a needle Jacobian that describes tip motion due to needle base motion and a deformable finite element tissue model. However, their work does not explore the effect of tip asymmetry. In addition, Glozman and Shoham [7] analyzed needle paths for steering and obstacle avoidance, but did not model the bevel tip.

Our approach differs significantly from previous needle steering work because of the use of tip asymmetry. A primary advantage of our technique is that it does not require significant deformation of potentially sensitive tissues, thereby minimizing tissue damage. Tissue damage could result in changing material properties, making needle steering plans based on estimates of tissue properties inaccurate. We presented a nonholonomic model of needle steering and our preliminary experiments in [8]. Our group is also exploring reachability, stochastic modeling and probabilistic planning [12], as well as finite element modeling for planning paths around obstacles in deformable tissue [1]. In this paper, we report our efforts in the design of needle steering robots and the results of experiments to determine the effects of insertion velocity and bevel angle on steering.

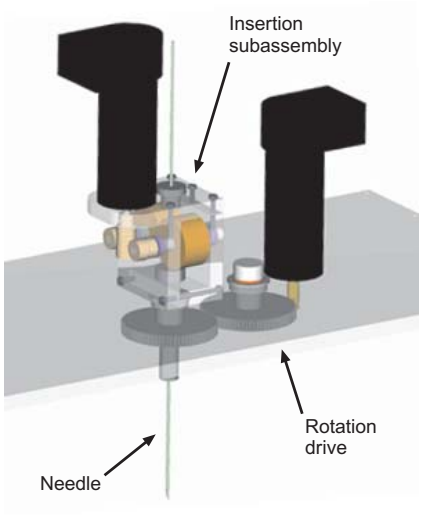

Fig. 1. CAD model of a friction drive needle insertion mechanism for steering of flexible needles.

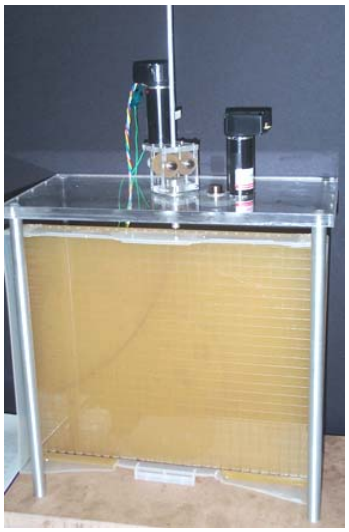

Fig. 2. Experimental setup using a friction drive needle insertion mechanism for steering of flexible needles.

II. Robotic Devices for Needle Steering

Automated flexible needle insertion is difficult because the needle will buckle if not supported near the tissue entry point. Humans are not able to insert a needle with a precise velocity, and they may inadvertently apply lateral forces or torque about the needle axis. In this section we examine two different robotic devices for steering needles using tip asymmetry. Each device is able to control insertion velocity and the rotation (spin about the needle axis) velocity. We do not consider devices for lateral motion of the base in this paper, but note that it can be easily achieved by mounting our devices on a higher degree-of-freedom manipulator, in order to provide a variety of needle steering methods.

A. Friction Drive Device

The first device designed was based on a friction drive concept. There have been other needle insertion devices incorporating friction drive, most notably a novel robot for percutaneous access to the kidney (PAKY) [14]. In that system, the goal was to provide a radiolucent driving mechanism and direct control of only insertion velocity. Our system consists of a friction-drive insertion subassembly, which is then rotated to generate spin about the needle axis. The device is shown in Figures 1 and 2.

In this device, the insertion subassembly drives the needle by grasping it on the barrel using two opposing rubber wheels actuated by a worm gear attached to a motor. Rotation of the needle about its axis is achieved by rotating the insertion subassembly as a unit. Since the wheels grasp the needle tightly by the barrel, rotating the subassembly causes the needle to rotate as well. A slotted needle guide (shown only in Figure 2) further fixes the orientation of base of the needle, and thus the bevel direction, relative to the drive wheels. This mitigates unwanted needle rotation as the drive wheels turn. Buckling is prevented by passing the needle through a 1.5 mm hole drilled through the aluminum rod that supports the insertion subassembly. This rod extends to the surface of the phantom tissue into which the needle is inserted.

The main advantage of this mechanism is compactness and simplicity. However, after preliminary experiments [8], we found three drawbacks to this design. First, the friction drive results in some linear slippage (generally small, but proportional to phantom tissue stiffness and friction properties), which increases the further the needle is inserted because of increased surface area contact between the needle shaft and the tissue. It would be possible to encode the amount of slip of the needle separately from the insertion motor motion using a linear encoder, but this would add complexity to the design. Second, the needle can spin slightly during insertion because of uneven contact forces with the rubber drive wheels. (This spin is much more pronounced in [14], where there is effectively only one drive wheel.) Third, measurements of needle force and torque are difficult to obtain using this system. Such information is not only interesting for modeling and scientific purposes, but torque about the needle axis may be crucial for eventual clinical implementation. This is because a very flexible needle will also have a finite torsional stiffness, resulting in a difference in angle between the base (outside the tissue) and the needle tip (inside the tissue) when the base is rotated. Model-based planning and real-time control requires that we have an estimate of the tip spin angle, and torque sensing will facilitate this. Given these limitations, a second device was designed and used to perform the experiments presented in the remainder of this paper.

B. Telescoping Support Device

The second needle insertion device design involves driving the needle from the base while utilizing a telescoping

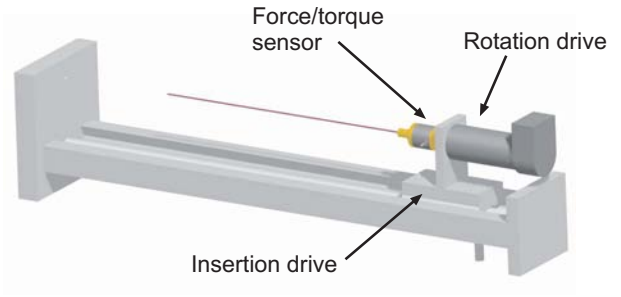

Fig. 3. CAD model of a mechanism that allows telescoping support (not pictured) for steering of flexible needles.

support sheath to prevent the needle from buckling. In this device, a needle rotation subassembly is moved by a translational stage, as shown in Figure 3. The needle is attached to the motor controlling spin about the needle axis through a Nano-17 ATI force/torque sensor (Figure 4). This allows us to measure two important quantities for tissue identification and steering control: the force along the needle axis and the torque about the needle axis. The translational stage used for linear insertion is a Velmex MA2524 linear stage with 20.5 inches of travel and a 2.5 turns/inch lead screw. It is actuated via a VEXTA PK266-03A stepper motor, which is operated by a Velmex VXM-1 controller.

The telescoping support sheath is created from the five segments of a disassembled radio antenna. Removing the friction couplings between the different segments results in a very low friction device. Figure 5 shows the antenna segments compressed near the entry point of the tissue. The inner diameter of the largest segment is 5.5 mm, while the inner diameter of the smallest segment is 2.3 mm. This smallest segment is inserted a short distance into a block of black Delrin (also shown in Figure 5) with a 1.0 mm hole, through which the needle passes after leaving the smallest section of the telescope and prior to entering the phantom tissue. This tight tolerance delivers the 0.83 mm diameter needle normal to the surface of the phantom tissue yet does not apply significant frictional forces. The friction force between the segments of the telescope was not measurable until the needle had been inserted a long distance into the tissue. When friction on the barrel of the needle presents enough of an opposing force to needle motion, the needle presses against the telescope wall with enough force to noticeably increase the friction of the telescope sections sliding over each other. However, this does not result in any visible deformation of the telescoping support. Figure 6 shows the experimental setup using this needle insertion device.

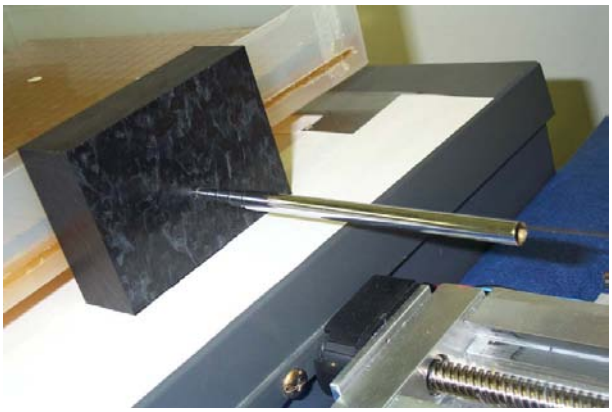

Fig. 5. Close view of the telescoping support sheath, shown in a compressed view to expose the the needle. The 1.0 mm hole in the black Delrin block serves as the smallest section of the support sheath, and ensures that the needle is introduced normal to the tissue surface.

III. Experiment Design Considerations

In addition to appropriate robotic mechanisms, accurate needle steering experiments require careful selection of needle and phantom tissue materials, calibration methods, and needle tracking algorithms. We note that although the experiments presented here are essentially planar, this system has the capability for three-dimensional experiments.

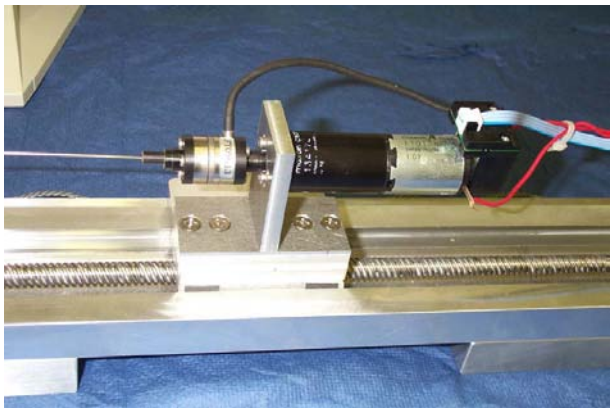

Fig. 4. Close view of the needle rotation mechanism. A 6-axis force/torque sensor is placed between the needle and the drive motor.

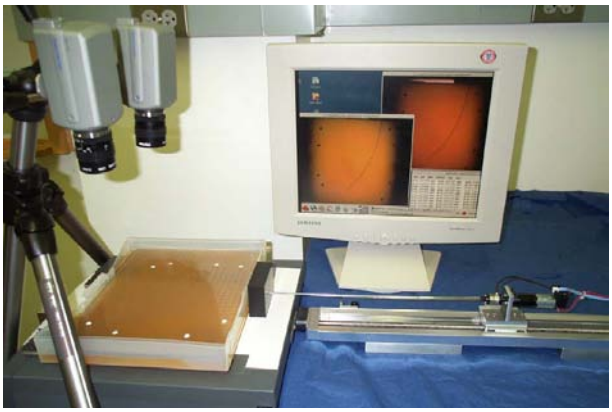

Fig. 6. Experimental setup using a telescoping support needle insertion mechanism for steering flexible needles.

A. Needle and Phantom Tissue Selection

The amount of needle bending is related to the material properties of the needle shaft, bevel angle of the needle tip, material properties of the phantom tissue, and friction forces between the surface of the needle and the surrounding tissue. The ideal phantom tissue would closely approximate the material properties of human tissue. While there have been some serious attempts to measure human tissue properties, the data is difficult to collect because the properties of ex vivo tissues differ greatly from those in living animals [3], [10]. Added to measurement difficulties is the challenge of re-creating the measured properties in a phantom tissue. Due to these issues, phantom tissues demonstrated to approximate all or nearly all properties of live human tissues do not exist today. However, there do exist some attempts to replicate certain individual elements of human tissue. One of these is the Simulated Muscle Ballistic Test Media from Corbin, Inc. This rubber-like simulated muscle is particularly useful for needle insertion because it is fairly stiff (4.9 N/mm by a blunt indentation test), and yet has a comparatively lower friction on the barrel of the needle than many alternative phantom tissues (such as silicone) of similar stiffness. While stiffer than most human soft tissue, the stiffness of the phantom material was useful for generating a significant amount of bending in Nitinol needles of the diameter commonly used in surgical procedures.

The needle used in our experiments was a 0.83 mm diameter solid Nitinol cylinder (simulating a 21 gauge needle) with a smooth surface finish and a hand-machined bevel tip. Nitinol is an alloy of approximately 55% Nickel and 45% Titanium, which becomes a superelastic material when properly heat treated. The Nitinol cylinder used in these experiments was obtained from Nitinol Devices and Components (NDC).

The Simulated Muscle was cast into a sheet approximately 15 mm thick, and the needle was introduced horizontally, using the telescoping support device described previously. In the experiments presented here, macroscopic displacement of the tissue by the needle did not occur. That is to say, the needle shaft followed and remained approximately fixed in the path the tip cut through the rubber as shown in Figure 7.

B. Calibration of Needle Insertion Angle

One of the most difficult practical considerations in attempting planar experiments was initial calibration of the orientation of the bevel tip about the needle axis. The needle diameter is small enough that it is difficult to accurately orient the bevel angle (Figure 8) by eye – especially considering that even a few degrees of error in initial rotation can cause the needle to move out of plane a distance greater than the thickness of the rubber sheet over the course of a 25 cm insertion. One way to ensure that the bevel is pointing in the plane of the rubber is to rotate it as well as possible by eye, and then insert it several times observing the direction of out of plane motion and correcting by rotating the needle a few degrees in the appropriate direction until the needle can be inserted to its full depth without going out of plane more than a few millimeters.

Fig. 7. Tip positions during needle insertion shown overlaid on the final needle path. Tip positions were extracted automatically from insertion images.

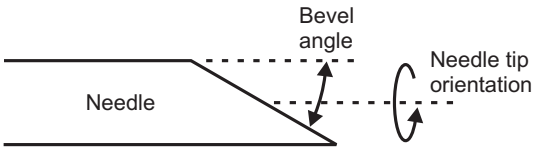

Fig. 8. Definition of the bevel tip angle and needle orientation.

C. Needle Tracking

Visual image data for each needle insertion is captured using stereo cameras placed approximately 0.8 m above the horizontal surface of the tissue phantom. The cameras used were Sony DFW-V500 digital firewire cameras, and provided 640x480 pixel images at a rate of 7.5 frames per second during each needle insertion.

To track the needle tip through the phantom, subsequent images are subtracted from each other, yielding difference images that are empty aside from a group of pixels indicating the change in needle tip position between the two images. These images are then converted to black and white using a threshold value that allows the needle tip pixels to show clearly. Connected pixels were then identified in order to locate the tip 'blob', and the lowest pixel in the blob corresponding to the direction of the tip was identified as the needle position for that pair of images. Repeating this process many times with subsequent images yields the

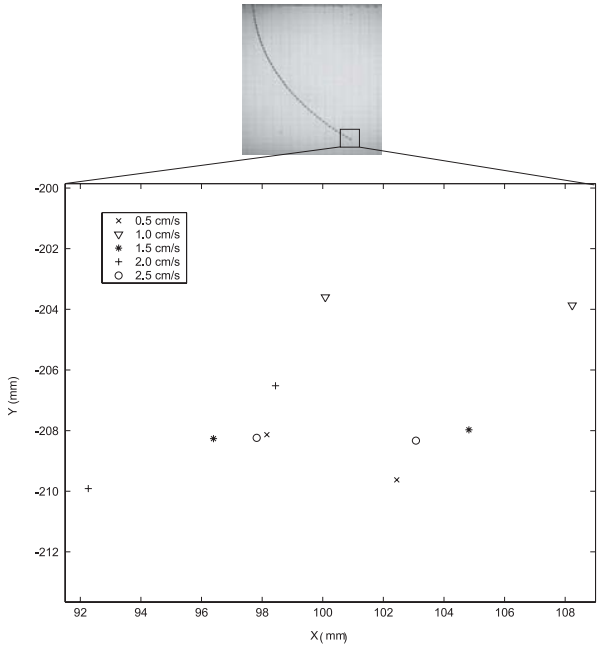

Fig. 9. A scatter plot of final needle tip positions for the velocity experiment. No trend is apparent.

needle path as shown by the dots superimposed on the final needle image in Figure 7.

When corresponding points on the needle in the left and right camera images have been identified according to the needle tracking algorithm above, the 3D coordinates of these points can be found by stereo triangulation. Stereo triangulation requires calibration of the stereo camera system, which was carried using the algorithms included in the Camera Calibration Toolbox for Matlab [2]. This procedure yields the transformation between the two cameras as well as the intrinsic properties of each. When a point is triangulated, the result is that point expressed in one of the camera coordinate frames. However, for intuition about the position of this point, it is useful to express the point in a coordinate frame attached to the phantom tissue surface with two axes parallel to it. To obtain the transformation between a camera frame and this phantom frame, the H-Matrix method was used. A 1 cm square grid was overlayed on the surface of the phantom tissue and 22 corresponding points were selected from the left and right images by clicking on grid intersections. Since these points were known in both the camera coordinate frame and the phantom coordinate frame, the H-matrix method yields the transformation between the two.

IV. Effect of Insertion Velocity

Using the system design described above, experiments were performed to determine the effect of insertion velocity on needle bending and axial forces.

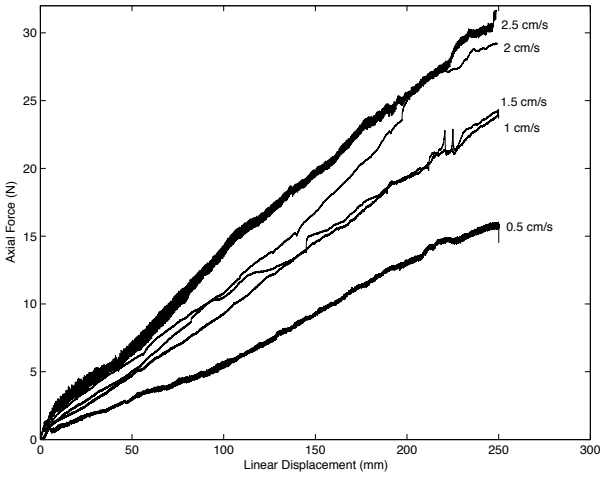

Fig. 10. Axial forces for runs with different velocities showing increased forces with increasing velocity.

A. Method

The effect of velocity on needle bending was studied by inserting the needle multiple times into a single rubber sample at velocities from 0.5 to 2.5 cm/s in increments of 0.5 cm/s. Care was taken that the needle was not inserted repeatedly at the same location, so the path cut by each insertion would have no effect on other insertions. The needle used in this experiment had a hand-machined bevel angle of $40°$. Each velocity was run twice, and the insertion distance for all runs was 25 cm.

The resulting tip and base positions were triangulated and expressed in the phantom coordinate frame as described previously. The various needle paths were shifted so that they had a common starting point. Some runs were performed with the bevel tip facing to the right and some to the left, so the "left" data sets were reflected about the y-z plane of the phantom coordinate frame so that they could be compared directly to the "right" data sets.

B. Path effects

The results of the velocity experiment are plotted in Figure 9. As can be seen from the figure, there is no discernable trend in the final tip location of the needles for the different velocities. This indicates that for our choices of phantom material and needle, viscous effects are negligible.

C. Force effects

Velocity did have an effect on the force required to drive the needle into the tissue. Figure 10 indicates that as the velocity increases, the force required to insert the needle also increases. The variability of the force data changes at different velocities – some of the plots are smoother than others. The reason for this is the mechanical resonance of the linear stage–stepper motor combination used for insertion. At velocities close to its resonances it tends to

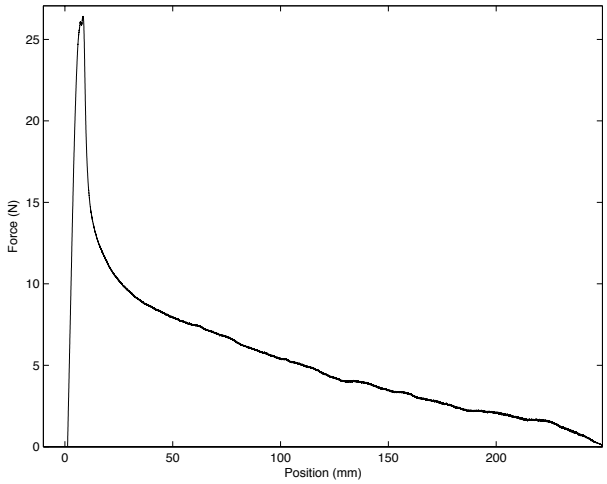

Fig. 11. Example retraction forces.

vibrate more, causing corresponding vibrations in the force readings. The forces measured as the needle is removed from the tissue (Figure 11) are as one would expect. The needle first overcomes static friction, and then the effects of kinetic friction are evident and shrink as the the amount of needle embedded in the tissue decreases.

V. Effect of Bevel Tip Angle

Since the asymmetry of the bevel tip provides steering actuation forces, it is reasonable to believe that different bevel angles will result in different needle paths for the same insertion parameters. At the theoretical extremes, a 90° bevel should provide no bending and a 0° bevel would cause the needle to have the most bending. The goal of the experiments in this section is to validate this hypothesis and test the effect of a wide range of practical bevel angles on needle steerability.

A. Method

The effect of the bevel tip angle on needle bending was studied by inserting the same needle multiple times into a single rubber sample. Between each insertion, a different bevel angle was ground onto the needle tip. The angles used, measured as indicated in Figure 8, were $5°$, $25°$, $40°$, $60°$, and $80°$. As in the velocity experiment, care was taken that the needle was not inserted at the same location twice. The needle was inserted for each run at a constant velocity of 1.5 cm/s. Each bevel angle was run twice, and all runs were for an insertion distance of 22 cm. The resulting tip positions were triangulated and compared as in the velocity experiment.

B. Path effects

The results of the bevel tip experiment are shown in Figure 12. As can be seen in the figure, there is a trend in the amount of bending obtained from the different bevel angles, with 5° producing the most bending and 80° the least. Note that the range of bending in the x direction between the different bevel angles is approximately 2.5 cm, or over 10% of the total insertion distance. The final positions of the entire needle for all 5 bevel angles are shown in Figure 13.

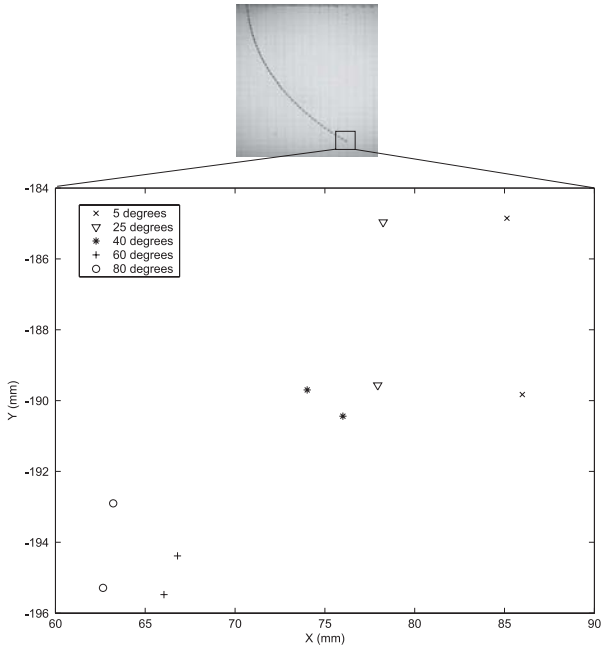

Fig. 12. A scatter plot of final needle tip positions for the velocity experiment.

Fig. 13. The final needle locations, extracted from difference images, with different bevel angles illustrate the steering effect of the bevel tip. A 5° bevel exhibits the most bending while an 80° bevel the least.

C. Force effects

Figure 14 shows that there is little difference in the axial forces on the needle for different bevel tip angles, as compared with the effect of velocity (Figure 10). This indicates that the friction forces on the barrel of the needle tend to dominate the cutting force of the needle tip. The sudden jumps in force near the end of the runs indicate situations

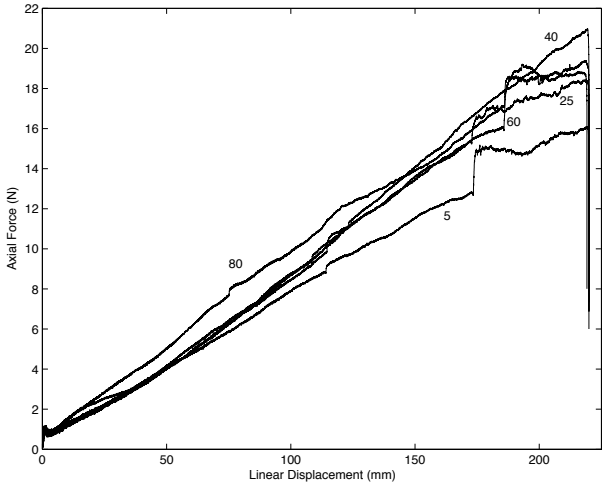

Fig. 14. Axial forces for runs with different bevel angles.

when the needle pressed on the wall of the telescope hard enough to cause a significant increase in its friction. The tangential forces (not plotted here) yield little information, because the telescope and the Delrin block mask them from being accurately sensed by the force sensor. Torque data did not provide any significant information because the needle was not rotated about its axis during the insertions. In more complicated 3D trajectories, torque may be used to help derive needle tip orientation.

VI. Conclusion

This paper presented devices and design considerations for steering flexible needles using bevel tips. For device design, it was found that a friction drive robot was compact and simple, yet presented some issues with drive wheel slippage and force sensor integration. A robotic device with a telescoping support sheath was found effective at preventing needle buckling, and allowed force/torque measurement to our maximum experimental insertion depth of 22-25 cm. An experimental setup for needle steering must take into consideration phantom and needle material properties, initial needle insertion angle, and stereo computer vision tracking issues.

Our experimental results indicate that bevel angle has an effect on needle steering and that down to 5° (the steepest reasonable bevel angle we produced) steering was monotonically increasing with decreasing angle, and that we could produce a significant change in final tip position between a 5° bevel and an 80° bevel.

However, we found that the speed of needle insertion in the homogeneous, relatively stiff phantom tissue we used had no discernable effect on steering. This may change with phantom tissues more representative of living human tissue, since damping and puncture events may be present.

In future work, we will examine the application of needle steering experiments to more realistic settings, using phantom tissue with deformation and layers/membranes. In addition, we will need to consider the tracking of 3D needle insertions (here they were primarily planar). This will be facilitated by obtaining a more transparent phantom tissue, and possibly placing marks (such as stripes) on the needle that will aid in segmentation of the needle in the images. Ultimately the needle will be tracked in real, in vivo, opaque tissue using biplane x-ray.

Acknowledgment

The authors thank Noah Cowan, Jessica Crouch, and Panadda Marayong for their advice regarding image capture and processing.

References

[1] R. Alterovitz and K. Goldberg. Planning for steerable bevel-yip needle insertion through 2d soft tissue with obstacles. *IEEE International Conference on Robotics and Automation*, 2005. Submitted.

[2] J.-Y. Bouguet. Camera calibration toolbox for matlab. `http://www.vision.caltech.edu/bouguetj/calib_doc/index.html`. Last acessed September 2004.

[3] I. Brouwer, J. Ustin, L. Bentley, A. Sherman, N. Dhruv, and F. Tendick. Measuring in vivo animal soft tissue properties for haptic modeling in surgical simulation. *Medicine Meets Virtual Reality*, pages 69–74, 2001.

[4] W. Daum. A deflectable needle assembly, 2003. Patent 5,572,593.

[5] S. P. DiMaio and S. E. Salcudean. Needle steering and model-based trajectory planning. *Medical Image Computing and Computer-Assisted Intervention*, pages 33–40, 2003.

[6] R. Ebrahimi, S. Okzawa, R. Rohling, and S. E. Salcudean. Hand-held steerable needle device. *Medical Image Computing and Computer-Assisted Intervention*, pages 223–230, 2003.

[7] D. Glozman and M. Shoham. Flexible needle steering and optimal trajectory planning for percutaneous therapies. *Medical Image Computing and Computer-Assisted Intervention*, 2004.

[8] R. J. Webster III, N. J. Cowan, G. S. Chirikjian, and A. M. Okamura. Nonholonomic modeling of needle steering. *9th International Symposium on Experimental Robotics*, 2005. In press.

[9] H. Kataoka, T. Washio, M. Audette, and K. Mizuhara. A model for relations between needle deflection, force, and thickness on penetration. *Medical Image Computing and Computer-Assisted Intervention*, pages 966–974, 2001.

[10] A. E. Kerdok and R. D. Howe. A technique for measuring mechanical properties of perfused solid organs. *ASME Summer Bioengineering Conference*, 2003.

[11] M. D. O'Leary, C. Simone, T. Washio, K. Yoshinaka, and A. M. Okamura. Robotic needle insertion: Effects of friction and needle geometry. *IEEE International Conference on Robotics and Automation*, 2003. In press.

[12] W. Park, J. S. Kim, Y. Zhou, N. J. Cowan, A. M. Okamura, and G. S. Chirikjian. Diffusion-based motion planning for a nonholonomic flexible needle model. *IEEE International Conference on Robotics and Automation*, 2005. Submitted.

[13] D. Song. Personal communication, 2003. Johns Hopkins Medical Instuitions, Division of Radiation Oncology.

[14] D. Stoianovici, J. A. Cadeddu, R. D. Demaree, S. A. Basile, R. H. Taylor, L. L. Whitcomb, W. N. Sharpe, and L. R. Kavoussi. A novel mechanical transmission applied to percutaneous renal access. *American Society of Mechanical Engineers Dynamic Systems and Control*, DSC 61:401–406, 1997.